Modeling study of impacts on surface ozone of regional transport and emission reductions over North China Plain in summer 2015

Xiao Han[1, 2], Lingyun Zhu[3], Shulan Wang[4], Xiaoyan Meng[5], Meigen Zhang[1, 2], Jun Hu[4]

[1] *State Key Laboratory of Atmospheric Boundary Layer Physics and Atmospheric Chemistry, Institute of Atmospheric Physics, Chinese Academy of Sciences, Beijing 100029, China.*

[2] *College of Earth Science, University of Chinese Academy of Sciences, Beijing 100049, China*

[3] *Shanxi Province Institute of Meteorological Sciences, Taiyuan 030002, China*

[4] *Chinese Research Academy of Environmental Sciences, Beijing, 100012, China*

[5] *China National Environmental Monitoring Centre, Beijing, 100012, China*

Corresponding author:

Meigen Zhang

LAPC, Institute of Atmospheric Physics, Chinese Academy of Sciences

HuaYanBeiLi 40#, Chaoyang District

Beijing, China

Post code: 100029

Tel: 86-010-62379620

Fax: 86-010-62041393

E-mail: mgzhang@mail.iap.ac.cn

Lingyun Zhu

E-mail: mgzhang@mail.iap.ac.cn

Other authors:

Xiao Han, E-mail: hanxiao@mail.iap.ac.cn

Shulan Wang, E-mail: shulanwang@foxmail.com

Xiaoyan Meng, E-mail: mengxy@cnemc.cn

Jun Hu, E-mail: hujun@craes.org.cn

Abstract

Tropospheric ozone (O_3) has replaced $PM_{2.5}$ or PM_{10} as the premier pollution in the North China Plain (NCP) during summer in recent years. A comprehensive understanding of the O_3 production in responding to the reduction of precursor emission over NCP is demanded urgently for the effective control policy design. In this study, the air quality modeling system RAMS-CMAQ (regional atmospheric modeling system-community multiscale air quality), coupled with the ISAM (integrated source apportionment method) module is applied to investigate the O_3 regional transport and source contribution features during a heavy O_3 pollution episode in June 2015 over NCP. The results show that the emission sources in Shandong and Hebei were the major contributors to O_3 production in the NCP. Not only the highest local contribution of O_3 mass burden, but also more than 30% contribution of O_3 mass burdens in Beijing and Tianjin were provided by the emission sources in these two provinces, respectively. On the other hand, the urban areas and most O_3 pollution regions of NCP were mainly dominated by the VOC-sensitive conditions, while "both control" and NO_x-sensitive conditions dominated the suburban and remote areas, respectively. Then, based on the sensitivity tests, the effects of several hypothetical scenarios of emission control on reducing the O_3 pollution were compared and discussed. The results indicated that the emission control of industry and residential sectors was the most efficient way if the emission reduction percentage was higher than 40%. However, when the emission reduction percentage dropped below 30%, the power plant sector could make significant contributions to the decrease in O_3. The control strategies should be promptly adjusted based on the emission reduction, and the modeling system can provide valuable information for precisely choosing the emission sector combination to achieve better efficiency.

1. Introduction

In addition to the downward injection of stratospheric ozone (O_3), tropospheric O_3 is formed via a suite of photochemical reactions involving nitrogen oxides (NO_x), volatile organic compounds (VOCs), and sunlight. O_3 plays an important role in controlling the chemical composition and climate of the troposphere and harms vegetation and human health, especially in industrialized regions (Kleinman et al., 2002). In recent years, the emission of O_3 precursors, NO_x and VOCs, have increased substantially due to the economic growth, rapid population expansion, and urbanization in the North China Plain (NCP). During the summer, $PM_{2.5}$ or PM_{10} are replaced by O_3 as the premier pollution type in major urban areas (China Environmental Status Bulletin 2015).

Numerous studies have investigated the spatial and temporal distribution characteristics of O_3 in the NCP. Lin et al. (2008) analyzed the three-year observation data of the O_3 mixing ratio at a remote Global Atmosphere Watch site near Beijing and showed the seasonal variation features of the O_3 background value for the NCP. Tang et al. (2012) gathered two-year observation data of the O_3 mixing ratio for 22 sites (located in urban, rural, and coastal areas) during a field campaign in the NCP and coupled the data with the meteorological parameters from the WRF. The spatial and temporal variations of O_3 were through analyzed, and the O_3–NO_x–VOCs sensitivity was initially investigated in this study. Ran et al. (2012) and Dufour et al. (2010) compared the O_3 seasonal variation features in megacities between the NCP and southern China. On the other hand, several studies have applied the chemistry transport model system to reproduce the three-dimensional O_3 continuous distribution characteristic and discussed the sensitivity of O_3 to precursor emissions (Wang et al., 2012; Nie et al., 2014).

Because of the strong emission of air pollutants, widespread haze clouds caused by serious air pollution have occurred frequently over the NCP (Tao et al., 2012; Wang et al., 2013; Li et al., 2016; Zhou et al., 2017). Aiming to solve this problem, the government has executed strict emission control strategies in recent years (Gao et al., 2016), which have yielded an initial effect. As reported by the China Environmental Status Bulletin, the mass loadings of sulfur dioxide (SO_2), NO_2, $PM_{2.5}$, and PM_{10} steadily fell from 2013 to 2015. However, O_3 has become the only pollutant whose mass burden has continued to increase in the 74 experimental cities of China, and the mass concentration is expected to continue increasing (Deng et al., 2011). Therefore, there is an urgent need to prevent environmental and health hazards in the NCP resulting from the surface O_3.

As a secondary pollutant, although the basic features of surface O_3 in the NCP are well known from

measurement or modeling studies, understanding the chemical links between O_3 and its two main precursors, NO_x and VOC, is important for designing effective pollution reduction strategies (Castell et al., 2009). The chemical transport model is an indispensable method for resolving the above issue, as it can quantify the main physical and chemical mechanisms of pollutant formation and transport. Liu et al. (2010) used two process analysis modules (integrated process rates and integrated reaction rates) embedded in CMAQ to capture the dynamical and photochemical processes of O_3 formation in 2008 over China. As a result, the influence and contribution of each important process can be distinguished and quantified. Tang et al. (2017) also used the integrated process rates module for measurement data from a set of observation stations to evaluate the sensitivity of O_3 production in June 2008 over the NCP. Xing et al. (2010) developed a statistical response surface method which aimed at investigating ozone sensitivities to NO_x and VOC emission changes and coupled it with CMAQ to analyze O_3 sensitivities to NO_x and VOCs emission changes in 2005 over eastern China. The overall impacts from individual sources, including regional NO_x and VOCs emission sources, have been evaluated using this modeling system. Li et al. (2008) applied a tagged tracer method to the framework of NAQPMS to identify the transport contributions from various O_3 production regions to total O_3 levels in 2008 over central eastern China. This method can be used to eliminate the errors caused by nonlinearities in the transport and fast photochemistry of O_3 and its precursors.

In general, the substantial features of O_3 formation sensitivity and the contributions of regional-scale transport have been discussed in these studies. However, more work needs to be done to achieve a comprehensive understanding of O_3 behavior over the NCP, especially the source contribution approaches of recent years. In this study, an air quality modeling system called RAMS-CMAQ (regional atmospheric modeling system–community multiscale air quality) that is coupled with the ISAM (integrated source apportionment method) module is applied to estimate the regional contributions of O_3 among major regions of the NCP and to quantify the relative amount of O_3 originating from specific VOCs and NO_x emissions sources. A unique method that can distinguish the O_3–NO_x–VOC sensitivity features is also used to identify the precursor sensitivity regions and verify the results of the ISAM. In addition, the brute-force method is applied to investigate the effect of reducing anthropogenic emissions on the O_3 mass burden. Therefore, the precursor control type and contribution from specific geographic areas and emission sectors can be obtained, and some valuable information can be provided for control strategies in the NCP.

2. Methodology

CMAQ (version 5.0.2), released in April 2014 by the US EPA (https://www.airqualitymodeling.org/index.php?title=CMAQ_version_5.0.2_(April_2014_release)_Technical_Documentation&oldid=587), was applied over the NCP for 2-month simulations in January and June 2015. Several updates and revisions, such as the chemical process corresponding to NH_3 and SO_2 and the secondary aerosol formation of SOA (secondary organic aerosol) and nitrate, have been added in this version. The updated and expanded version of the carbon bond mechanism (CB05) (Sarwar et al., 2008) and the sixth-generation modal CMAQ aerosol model (AERO6) were applied to simulate the gas-phase chemistry mechanisms and formation and the dynamic processes of aerosols, respectively. The ISORROPIA model (version 1.7) was used to describe the thermodynamic equilibrium of gas-particle transformation (Nenes et al., 1999). The highly versatile RAMS numerical code (Cotton et al., 2003), which can well simulate the boundary layer and the underlying surface, is utilized to provide the meteorological fields for CMAQ. The mechanisms about secondary organic aerosol formation, on-line dust emission were modified for improving the simulation ability in China (Han et al., 2012; Li et al., 2017), and the information of underlying surface in China was also updated (Chen et al., 2018).

The anthropogenic emissions of major pollution species (NO_x, SO_2, VOCs, BC, OC, primary $PM_{2.5}$, and PM_{10}) were obtained from the monthly-based emission inventory, with 0.25°×0.25° horizontal resolution and four categories (industry, power, transport, and residential), which were developed to support the Model Intercomparison Study Asia (Li et al., 2015). The original version of this emission inventory was developed for Asia as a contribution to the TRACE-P (Transport and Chemical Evolution over the Pacific) Mission and ACE-Asia (Asian Pacific Regional Aerosol Characterization Experiment) (Streets et al., 2003). Additionally, the NO_x and NH_3 emissions from the soil and natural hydrocarbon emissions were obtained from the Global Emissions Inventory Activity 1°×1° global monthly inventory (Benkovitz et al., 1996). The Global Fire Emissions Database, Version 3 (FGEDv3.0; van der Werf et al., 2010), was applied to provide the biomass burning emissions from wildfires, savanna burning, and slash-and-burn agriculture. The VOCs and nitrogen oxides from flight exhaust, lighting, paint, fossil fuel, and other sectors were obtained from the regional emission inventory in Asia (REAS, Version 2, http://www.jamstec.go.jp/frsgc/research/d4/emission.htm) and the emission database for global atmospheric research (Olivier et al., 1994), respectively.

The ISAM module was used to track O_3 from different geographic regions and source types. This

source apportionment tool was developed from the TSSA (tagged species source apportionment; Wang et al., 2009) in an early version of the CMAQ model. Compared with the previous version, the ISAM improved the approach for the advection of tagged tracers and the tracking of precursor reactions and increased the flexibility of the application by minimizing the amount of data preparation (Kwok et al., 2013). An updated piecewise parabolic algorithm was applied to reasonably estimate the major dynamics processes, including advection transport, vertical diffusion, and dry deposition. For the nonlinear gas-phase chemical interactions, which are important for O_3 formation, a hybrid approach that employs the direct sensitivity methods as linear equations using lower and upper triangular matrices, which is known as LU decomposition (Yang et al., 1997), was applied for description. In addition, the ISAM uses two tracers for individual nitrogen and VOC species to represent the O_3 chemical formation regime attributed to either NO_x or VOC emission sources. As described by Kwok et al. (2014), the total concentration of O_3 in each model grid cell is equal to the sum of O_3 tracers that were produced in either VOC- or NO_x-sensitive conditions:

$$O_{3\,bulk} = \sum_{tag} O_3V_{tag} + \sum_{tag} O_3N_{tag} \quad (1)$$

where O_3V_{tag} and O_3N_{tag} are the VOC-sensitive and NO_x-sensitive O_3 attributed to each tag source, respectively. Therefore, the contribution from VOCs or NO_x can be tracked individually, and the precursor control types in each grid can be deduced. Detailed information regarding the ISAM can be found in Kwok et al. (2013).

The simulation has two layer grids. The coarse domain covers East Asia (Figure 1, D1), with a horizontal grid spacing of 64 km and a total area of 6654 km×5440 km, and an inner domain (Figure 1, D2) with a 16 km×16 km resolution is two-way nested with the outer one. The inner domain covers the major regions of the NCP, including the megacity of Beijing, Tianjin, the capital city of the Shijiazhuang province, Jinan, the industrial town of Tangshan, and the Hebei, Shandong, and Shanxi provinces. The simulation used 15 vertical levels, of which nearly half were concentrated in the lowest 2 km, to improve the simulation of the atmospheric boundary layer. Numerous previous studies have demonstrated that this modeling system performs well in simulating the pollutant mass concentrations (Zhang et al., 2006; Han et al., 2014; Han et al., 2016)

3. Model evaluation

The meteorological parameters, such as the temperature and wind field, are important impact factors

of ozone formation and transport. Therefore, the daily average temperature, relative humidity, wind speed, and maximum wind direction in January and June 2015 were compared with the surface observation data (released by the Chinese National Meteorological Center: http://data.cma.cn/) for Beijing, Tianjin, Shijiazhuang, and Jinan. The comparison results are shown in Figure 2. The modeled temperature and relative humidity are shown to generally coincide with the observations at all four of these stations, except that some of the extreme high or low values appeared abruptly. The modeled wind speed, which could reproduce the higher value in Tianjin and Jinan and lower value in Beijing and Shijiazhuang, also followed the magnitude of observations well. However, a direct comparison between observed and modeled data is difficult, especially for the wind direction. Besides the obviously impact of surrounding surface at each measurement station, the time resolutions between observation (10 minute mean) and model output (1 hour) were also different. Nevertheless, the north wind in winter and south wind in summer were generally captured by the simulation results for all stations.

The modeled mass concentrations of O_3 and one of its precursors (NO_2) were compared with the hourly observation data from the Ministry of Environmental Protection of China; the results are shown in Figures 3 and 4. The statistical parameters the means, standard deviation, and correlation coefficients between the observations and simulations are listed in Tables 1 and 2. The nitrogen oxide and tropospheric ozone were two kinds of typical trace gases with high chemical activity and relatively short lifetimes. The diurnal change in Figures 3 and 4 is obvious, and the distinctive values of the mass concentrations between different seasons can also be found. The simulation results also reproduced these important features, especially the evident diurnal variation of O_3 at these four stations. The mass concentration of O_3 in summer was generally higher than that in winter because of the strong photochemistry during the daytime in summer. On the other hand, the metrics listed in Tables 1 and 2 were used to evaluate the model performance, following the study of Yu et al. (2006). Most of the correlation coefficients were higher than 0.5 for NO_2 and 0.6 for O_3, which indicates that the model performed well in reproducing the observation trend. The simulation results were able to capture most of the pollution episodes during these two months. In addition, the standard deviations between the observation and simulation of NO_2 and O_3 were also similar in most cases. Most of the mean NO_2 concentration of simulation was generally similar with that of the observation in June, but about 25 $\mu g\ m^{-3}$ lower at Tianjin in January. As shown in Figure 3, the model missed some of the high values of observation that appeared during the first half of January. The largest deviation of the modeled O_3, which the mean mass burden was obviously higher than that of the observation and the correlation coefficient was

just 0.48, also appeared at Tianjin in January. Yu et al. (2010) reported similar results and noted that the model might not well resolve the titration by NO in an urban area under a low O_3 mass burden background by applying both the CB05 and SAPRC-99 mechanisms. Nevertheless, the comparison generally showed that the model could basically reproduce the meteorological field and mass concentration and trends of O_3 and its precursor NO_2 during different seasons over the NCP.

4. Results and discussion

The surface spatial distributions of the monthly average values of the modeled NO_x, VOCs, and maximum daily 8-hour average O_3 mass concentration (8H-O_3) for January and June 2015 are shown in Figure 5. The monthly average wind field is also shown. The diffusion condition is shown to have been weak due to the obviously smaller wind speed over Beijing, Tianjin, Hebei, Shandong, and northern Henan in both January and June. In addition to the strong emission, the weak diffusion condition should be the main reason for the high mass burden of NO_x and VOCs in these regions. In addition, the maximum values were mainly concentrated in the urban areas of the NCP during these two months, including the following five major pollution cities: Beijing, Tianjin, Shijiazhuang, Jinan, and Tangshan. However, the distribution patterns between O_3 and the precursors were significantly different, which indicates that the formation and transport processes of O_3 should be complex in the NCP. Unlike the seasonal variation of NO_x and VOCs, the mass burden of O_3 in summer was obviously higher than that in winter because of the stronger photochemical activity. The 8H-O_3 mass concentration, which exceeded the Grade II standard (160 μg m^{-3}), was widespread throughout southern Beijing, Hebei and almost the entire areas of Tianjin and Shandong, with values reaching 180-200 μg m^{-3} in the tri-province area of Hebei, Shandong, and Henan in June. The serious O_3 pollution was mainly concentrated in the northwest part of the Shandong province.

The contribution of O_3 from the major NCP regions, including Beijing, Hebei, Shandong, Tianjin, and Shanxi, was calculated using ISAM-CMAQ-RAMS; the results are shown in Figure 6 (NS: NO_x-sensitive O_3) and Figure 7 (VS: VOC-sensitive O_3). The total percentage can be obtained by summing the contributors of NS and VS and shown in Table 3. The distribution patterns of NS and VS contributions were generally similar to each other. The mass contribution of O_3 in Shandong, Hebei, and Shanxi was mainly provided by local anthropogenic sources, and the local contribution could reach 36.6%, 53.6%, and 45.0%. However, the local sources did not provide the primary contributions in Beijing (23.1%) and Tianjin (14.9%), and the regional transport contributions from Hebei and Shandong could reach 35.2% and 37.3%

to these two cities, respectively. This feature clearly indicates that the regional transport of precursors should be an important factor of O_3 pollution in Beijing and Tianjin. The contribution from Shanxi to other regions was very small due to the hindrance to pollutant transport caused by the Taihang Mountains, which are located to the east of the Shanxi province. The contribution from other regions to Shanxi was also very low in corresponding as shown in Table 3. In addition, the contribution from Shandong provided at least more than 65% to the mass burden of O_3 in the Bohai Sea. This feature explains the source of the large value that appears over this area in Figure 4. On the other hand, the contribution of VS was obviously higher than that of NS in Beijing, Tianjin, Hebei, and Shandong. Compared with the NS, the percentage of VS was generally double in Beijing and Tianjin and more than 10% higher in all of Shandong and the southern part of Hebei. In contrast, the contribution of NS was clearly higher than that of VS in Shanxi, which means that the major role of the O_3 formation in Shanxi should be different from that in other regions.

To distinguish the O_3–NO_x–VOC sensitivity features, a method that is suitable for the results of three-dimensional chemistry/transport models was applied to identify the precursor sensitivity regions in the NCP. In addition to the base case, two sensitivity tests, which reduced 30% of the VOC emissions and 30% of the NO_x emissions, respectively, within the entire model domain, were conducted. Then, the deviation of the maximum daily 8H-O_3 between the base case and these two sensitivity tests could be utilized to determine the precursor control types in each grid. Here, we used ΔO_{3V} and ΔO_{3N} to represent the variation of the mass concentration of O_3 due to the reduction in VOC or NO_x emission, respectively (Sillman and He, 2002; Sillman and West, 2009): (1) if the changes in ΔO_{3V} and ΔO_{3N} were both less than 4 μg m^{-3}, this grid was likely controlled by neither NO_x nor VOCs; (2) if ΔO_{3N} increased to a value greater than 4 μg m^{-3} and ΔO_{3V} decreased to a value less than 4 μg m^{-3}, this grid should be regarded as "NO_x titration"; (3) if ΔO_{3V} decreased by more than 4 μg m^{-3}, with this reduction being twice as large as the ΔO_{3N} reduction (or ΔO_{3N} increase), this grid was likely controlled by VOCs; (4) if ΔO_{3N} decreased by more than 4 μg m^{-3}, with the reduction being twice as large as the ΔO_{3V} reduction, this grid was likely controlled by NO_x; (5) if ΔO_{3N} and ΔO_{3V} both decreased by more than 4 μg m^{-3} and the ratio between them was less than 2:1 or 1:2, this grid was likely controlled by both NO_x and VOCs. Details regarding the identification explained above can be found in Figure 8(f). The frequency of precursor control types in each grid in June was determined and is shown in Figure 8(a-e). The NO_x titration scarcely appeared in the model domain. The frequency of the "no control" type entirely exceeded 50% over the background regions when the O_3 mass burden was lower than 120 μg m^{-3} and gradually decreased as the O_3 mass burden increased. Over the O_3 pollution areas, a

grid with a "no control"-type frequency higher than 10% was seldom found. Specific to the considered regions, the urban area of Beijing, Tianjin, Tangshan, southern Hebei, and northern and western Shandong were mainly under VOC control, while the outer suburb of Beijing, all of Shanxi, and northern Hebei were mainly under NO_x control. The "both control" type generally appeared in the transitional zone between NO_x and VOC control. Compared with the results shown in Figures 6 and 7, the distribution feature of NO_x and VOC contributions highly coincided with that of the O_3 precursor sensitivity types, which demonstrated that this method is reliable.

In addition to the contribution feature of emission sources estimated using the ISAM, the effect of reducing anthropogenic emissions on the O_3 mass burden was also necessary to learn because the formation of O_3 from NO_x and VOC emissions is a typical nonlinear process. The brute-force method, which can realistically capture the nonlinear processes of secondary pollutant formation, was applied. Therefore, several sensitivity tests were designed, as shown in Table 4. First, the zero-out (100% source removal) simulations of four major sectors, i.e., industry, power plants, transport, and residential (sensitivity tests ZI, ZP, ZT, and ZR, respectively), were conducted to evaluate the efficiency of emission reduction for different sources in the NCP. Figure 9 presents the results of the brute-force sensitivity tests and the NO_x and VOC emission flux of each major sector. The removal of the industry sector is shown to have been the most efficient way to decrease the O_3 mass burden, and the variation of 8H-O_3 between 20 and 30 μg m^{-3} was generally concentrated in the high mass concentration regions. The main reason is likely that the VOC emission flux of the industry sector was significantly higher than that of the other sectors. Removal of the residential sector could also decrease the O_3 mass burden in most of the VOC control regions due to its VOC emission flux being notably higher than that of NO_x. In contrast, removal of the transport and power plant sectors could not effectively reduce the O_3 mass burden and even increased the mass burden in high pollution areas, such as southern Beijing, Tianjin, Tangshan, southern Hebei, Jinan, and other parts of Shandong. The NO_x emission flux of these two kinds of sectors was clearly higher than that of VOCs, especially for the power plant sector. It also caused the 8H-O_3 mass burden to decrease by 5-10 μg m^{-3} in Shanxi as a result of the removal of the power plant sector. It can be deduced that the ambient NO_x mass burden should be plentiful and restrained the O_3 formation because of the reaction below:

$$O_3 + NO \rightarrow NO_2 + O_2 \quad (2)$$

Therefore, the environmental condition would be benefit for the O_3 formation when the NOx mass burden decrease due to power plant or transport sector removal. In summary, if we focus on the major pollution

302 regions of the NCP, including Beijing, Tianjin, Hebei, and Shandong, reduction of the industry and
303 residential emission sectors should be an effective way to control the O_3 mass burden during heavy O_3
304 pollution episodes.

305 In addition, the realistic pollution control strategies are supposed to be applied to a specific sector in
306 the high emission regions (HERs) and used to develop a comprehensive reduction scheme; thus, a detailed
307 analysis is necessary to investigate more accurate and practical strategies. Other than applying the simple
308 zero-out sensitivity test over entire objective regions, we selected the regions that include cities and towns
309 with high anthropogenic emission flux in the Beijing, Tianjin, Hebei, and Shandong (BTHS) region to more
310 accurately match real emission control. Figure 10 presents the selected regions and the emission flux of
311 NO_x and VOCs from the industry sector, residential sector, and multiple combinations. First, the change in
312 8H-O_3 mass concentration associated with the anthropogenic emission in selected regions (Figures 10(i)
313 and 10(j)) was compared with that in the entire BTHS region (sensitivity tests A20%-HERs and A20%-
314 BHTS), as shown in Figures 11(a) and 11(b), respectively. The distribution patterns of the 8H-O_3 mass
315 burden variation were notably similar to each other, and the positive and negative values generally appeared
316 in the same regions. However, the negative value in Figure 11(b) was clearly higher than that in Figure
317 11(a). This disparity indicates that significant overestimation of the O_3 mass burden variation might occur
318 when we conduct a brute-force sensitivity test with broad reductions in emissions in the entire objective
319 regions.

320 According to the results of the zero-out sensitivity tests, the industry and residential sectors were the
321 major emission sources of O_3, while the power plant sector did not benefit O_3 formation. Thus, the effects
322 of reducing these industry and residential sectors were estimated using the brute-force method with 20%
323 emission intensity in the selected regions of BTHS (Figures 10(a) and 10(b)). Figures 11(c) and 11(d) show
324 the variation of O_3 associated with the industry and residential emission sectors (sensitivity tests I20%-
325 HER and R20%-HER), respectively. The 8H-O_3 mass concentration could decrease by 10-12 μg m^{-3} in
326 most of Shandong, especially in the strong polluted regions shown in Figure 11(c). In contrast, the value
327 slightly increased in the urban areas of Shijiazhuang, Tianjin, and Tangshan. In Figure 5(f), the 8H-O_3 mass
328 burden was relatively lower in these regions. Thus, the O_3 mass burden can be decreased rapidly by
329 controlling the industry emissions under a heavy O_3 pollution background. Figure 11(d) shows that the 8H-
330 O_3 mass concentration decreased overall in BTHS, though the range was only 1-5 μg m^{-3}. The likely main
331 reason is that the emission of VOCs was higher than that of NO_x from the residential sector, while the

emission intensity from the residential sector was relatively lower than that from industry. The mass burden of O_3 can also be reduced by controlling the residential emissions in the urban areas of Shijiazhuang, Tianjin, and Tangshan.

In addition, the influence of different combinations of emission sectors in BTHS was discussed. Figures 11(e) and 11(f) present the change in 8H-O_3 mass concentration associated with a 20% emission intensity for both the industry and residential sectors (sensitivity test IR20%-HERs) and the industry, transport, and residential sectors (sensitivity test ITR20%-HERs), respectively. The O_3 mass burden generally decreased sharply in BTHS, as shown in Figure 11(e), especially in the regions of Shandong with heavy pollution. The range and magnitude of decrease can obviously be enhanced while considering the reduction of the transport sector, as shown in Figure 11(f). Notably, the mass concentration of 8H-O_3 could decrease from 180-200 μg m^{-3} to 160-180 μg m^{-3} in the polluted regions of BTHS. Compared with the zero-out sensitivity test in Figure 9, the decrease in 8H-O_3 mass burden in Figure 11(f) was still clearly lower than that of ZI. This deviation indicates that the contribution source from other regions except BTHS should also be important. Even though 80% of the emission intensity was removed, the reduction in 8H-O_3 mass concentration still barely exceeded 20 μg m^{-3} in the NCP, as shown in Figures 11(c), 11(d), and 11(e), which means that it was difficult to keep the O_3 mass burden under the Grade II standard by controlling only the industry and residential emission sectors in HERs.

Therefore, more brute-force sensitivity tests with HERs emissions varied from 50% to 0% were conducted. The regional average 8H-O_3 mass concentrations in Beijing, Tianjin, Shijiazhuang, Jinan, and Tangshan with changes in emission are shown in Figure 12. Three series of sensitivity tests were conducted: reduction of the IR (industry and residential), ITR (industry, transport, and residential) and All (industry, transport, power plant, and residential) emission sectors. As shown, the 8H-O_3 mass concentration was higher than 160 μg m^{-3} in all five cities, while the emission percentage was 100%. When the emissions reduced to 50%, the 8H-O_3 mass concentrations of these three series slightly decreased for Beijing, Tianjin, Tangshan, and Jinan but increased for Shijiazhuang. The decrease in 8H-O_3 mass concentration as a result of reducing the IR emission was similar to that of the ITR emission when the emissions were reduced from 50% to 40% for all five cities but was not significant when the reduction was less than 40%. The lines corresponding to the ITR and All emission sectors generally decreased coherently for these five cities when the emissions were reduced from 50% to 30%. However, the effect of the ITR reduction was obviously weaker than that of the All reduction when the reduction was less than 30%. The decrease in 8H-O_3 mass

362 burden exceeded 12 μg m^{-3} when the All emission reduction was least, and the air quality in all five of these
363 cities could reach the Grade II standard. This phenomenon indicated that the influence of the transport and
364 power plant emission sectors on the decrease in O_3 mainly occurred after removing 60% of the IR or 70%
365 of the ITR emission intensity, respectively. Thus, an emission control sequence for different sectors should
366 be considered when exploring more effective strategies.
367
368 **5. Conclusions**
369 In this study, an air quality modeling system referred to as RAMS-CMAQ was applied to simulate the
370 O_3 mass concentration, and several sensitivity tests were conducted to investigate the O_3 pollution and to
371 discuss the relationship between O_3 production and emission contributions over the NCP in January and
372 June of 2015. First, the modeled daily meteorological factors (temperature, relative humidity, and wind
373 field) and hourly mass concentrations of O_3 and its precursor NO_2 were compared with ground-based
374 observation data to evaluate the accuracy and reliability. The simulation results were generally good and
375 able to broadly capture the values and variation trend of the observation data. Focusing on the heavy O_3
376 pollution period in June, an advanced source apportionment tool called ISAM was coupled with RAMS-
377 CMAQ and applied to estimate the regional transport contributions, with individual tracers for nitrogen and
378 VOC species used to represent the O_3 chemical formation regime attributed to either NO_x or VOC emission
379 sources in the NCP. Then, a unique method that is suitable for three-dimensional chemistry/transport models
380 was used to distinguish the O_3–NO_x–VOC sensitivity features and identify the precursor sensitivity in each
381 grid of the model domain. Therefore, the O_3 mass burden sensitivities to NO_x and VOC emission changes
382 and the correlative regional transport contribution features among major anthropogenic source regions in
383 the NCP can be clearly investigated using these methods. In addition, several brute-force sensitivity tests
384 were conducted to discuss the role of the main anthropogenic emission sectors on reducing the O_3 mass
385 burden, and an attempt was made to provide valuable suggestions for exploring more effective strategies
386 for preventing O_3 pollution. The results are summarized as follows:
387 1. The simulation results show that the seasonal variation of O_3 was significant and that the heavy
388 mass burden of 8H-O_3, which exceeded the Grade II standard, generally occurred in southern Beijing, Hebei
389 and almost all of Tianjin and Shandong in June. The mass burden of 8H-O_3 reached 180-200 μg m^{-3} mainly
390 in the tri-province area of Hebei, Shandong, and Henan. The distribution pattern and seasonal variation of
391 8H-O_3 were obviously different from those of its precursors, which indicates that the formation and

transport processes of O_3 should be complex in the NCP.

2. The results of RAMS-CMAQ-ISAM show that the emission sources in Shandong and Hebei were the major contributors to O_3 production in the NCP. In addition to these two provinces, the O_3 mass burden in Beijing and Tianjin was also significant. The emissions from Hebei and Shandong contributed 15-20% and 5-10% to Beijing and 10-20% and 15-20% to Tianjin, respectively. However, the O_3 mass burden in these two provinces was generally contributed by the provinces themselves. The results also show that the contribution of VS was clearly higher than that of NS in Beijing, Tianjin, Hebei, and Shandong, which indicates that the O_3 mainly originated from VOC emission sources. On the other hand, the emission sources in the Shanxi province almost had no impact on the O_3 mass burden in other regions of the NCP due to the hinderance to pollutant transport provided by the Taihang Mountains.

3. The results of identification of the O_3–NO_x–VOC sensitivity feature show that the VOC control mainly occurred over all of Tianjin and Tangshan and southern Beijing (urban area) and Hebei, where the O_3 mass concentration reached 160-180 μg m^{-3}. The north central part of Shandong and urban area of Jinan were also mainly under the VOC control. The frequencies of VOC control and the "both control" type was generally equal in the region of Hebei and Shandong where the O_3 mass concentration reached 180-200 μg m^{-3}. The NO_x control generally appeared in the regions of the NCP where the O_3 mass concentration reached 120-160 μg m^{-3}. In the major cities with O_3 pollution, including Beijing, Tianjin, Shijiazhuang, and Jinan, the O_3–NO_x–VOC sensitivity feature was the same: VOC control dominated the urban area, while "both control" and NO_x control dominated the suburban and remote areas, respectively.

4. The results of the zero-out sensitivity tests show that the IR emission sectors were two important contributors to ozone formation, as they were the major sources of VOCs, while the power plant emission sector did not benefit O_3 pollution control in the high mass burden regions due to the greater emission of NO_x versus VOCs.

On the other hand, the results of the brute-force sensitivity tests show that the effects of IR, ITR, and All emission control on the decrease in O_3 were similar when their reduction percentages were higher than 40%. Meanwhile, the effects of ITR and All emission control were similar while the reduction percentages were higher than 30%. When the reduction percentage dropped below 30%, the nonlinearity of O_3 formation was notable, and the power plant sector could make significant contributions to the decrease in O_3. Thus, the control strategies should be promptly adjusted based on the emission reduction, and the emission sector combination should be precisely chosen to achieve better efficiency. The modeling system

allows us to capture valuable information regarding how to choose the correct sequence and efficient combinations by exploring the key thresholds from the bulk of sensitivity tests regarding crucial parameters.

References

Benkovitz, C. M., Schultz, M.T., Pacyna, J., Tarrason, L., Dignon, J., Voldner, E.C., Spiro, P.A., Logan, A., and Graedel, T.E.: Global gridded inventories of anthropogenic emissions of sulfur and nitrogen, J. Geophys. Res., 101(29), 239-253, 1996.

Castell, N., Stein, A., Mantilla, E., Salvador, R., and Millan, M.: Evaluation of the use of photochemical indicators to assess ozone-NO_x-VOC sensitivity in the Southwestern Iberian Peninsula, J. Atmos. Chem., 63(1), 73-91, 2009.

Chen, L., Zhang, M., Zhu. J., Wang, Y., Skorokhod, A.,: Modeling Impacts of Urbanization and Urban Heat Island Mitigation on Boundary Layer Meteorology and Air Quality in Beijing Under Different Weather Conditions, J. Geophys. Res., 123(8), 4323-4344, 2018.

Cotton, W. R., Pielke, R. A., Walko, R. L., Liston, G. E., Tremback, C. J., Jiang, H., McAnelly, R. L., Harrington, J. Y., Nicholls, M. E., Carrio, G. G., and McFadden, J. P.: RAMS 2001: current status and futures directions, Meteor. Atmos. Phys., 82, doi:10.1007/s00703-001-0584-9, 2003.

Deng, X., Zhou, X., Wu, D., Tie, X., Tan, H., Li, F., Bi, X., Deng, T., and Jiang, D.: Effect of atmospheric aerosol on surface ozone variation over the Pearl River Delta region, Sci. China Earth Sci., 54(5), 744-752, 2011.

Dufour, G., Fremenko, M., Orphai, J., and Flaud, J.: IASI observations of seasonal and day-to-day variations of tropospheric ozone over three highly populated areas of China: Beijing, Shanghai, and Hong Kong, Atmos. Chem. Phys., 10, 3787-3801, 2010.

Gao, W., Tang, G., Ji, D., and Wang, Y.: Implementation effects and countermeasures of China's air pollution prevention and control action plan, Res. Environ. Sci., 29(11), 1567-1574, 2016. (In Chinese)

Han, X., Ge, C., Tao, J., Zhang, M., Zhang, R.: Air Quality Modeling for a Strong Dust Event in East Asia in March 2010, Aerosol Air Qual. Res., 12: 615–628.

Han, X., Zhang, M., Gao, J., Wang, S., Chai, F.: Modeling analysis of the seasonal characteristics of haze formation in Beijing, Atmos. Chem. Phys., 14, 10231–10248, 2014.

Han, X., Zhang, M., Zhu, L., Skorokhod, A.: Assessment of the impact of emissions reductions on air quality over North China Plain, 7, 249-259, 2016.

Kleinman, L. I., Daum, P. H., Lee, Y. N., Nunnermacker, L. J., Springston, S. R., Lloyd, J., and Rudolph, J.: Ozone production efficiency in an urban area, J. Geophys. Res., 107, D23, 23, 2002.

Kwok, R. H. F., Baker, K. R., Napelenok, S. L., and Tonnesen, G. S.: Photochemical grid model implementation and application of VOC, NOx, and O3 source apportionment, Geosci. Model Dev., 7(5), 99-114, 2014.

Kwok, R., Napelenok, S., and Baker, K.: Implementation and evaluation of $PM_{2.5}$ source contribution analysis in a photochemical model, Atmos. Environ., 80, 398–407, 2013.

Li, H., Zhang, Q., Chen, C., Wang, L., Wei, Z., Zhou, S., Parworth, C., Zheng, B., Canonaco, F., Prevot, A., Chen, P., Zhang, H., and He, K.: Wintertime aerosol chemistry and haze evolution in an extremely polluted city of North China Plain: significant contribution from coal and biomass combustions, Atmos. Chem. Phys., 17, 4751-4768, 2017.

Li, J., Zhang, M., Wu, F., Sun, Y., Tang, G.: Assessment of the impacts of aromatic VOC emissions and yields of SOA on SOA concentrations with the air quality model RAMS-CMAQ, Atmos. Environ., 158, 105-115.

Li, M., Zhang, Q., Kurokawa, J., Woo, H., He, K., Lu, Z., Ohara, T., Song, Y., Streets, D., Carmichael, G., Cheng, Y., Huo, H., Liu, F., Su, H., and Zhang, B.: MIX: a mosaic Asian anthropogenic emission

inventory for the MICS-Asia and the HTAP projects, Atmos. Chem. Phys. Discuss, 15, 34813-34869, 2015.
Lin, W., Xu, X., Zhang, X., and Tang, J.: Contributions of pollutants from North China Plain to surface ozone at the Shangdianzi GAW Station, Atmos. Chem. Phys., 8, 5889-5898, 2008.
Liu, X., Zhang, Y., Xing, J., Zhang, Q., Wang, K., Streets, D., Jang, C., Wang, W., and Hao, J.: Understanding of regional air pollution over China using CMAQ, part II. Process analysis and sensitivity of ozone and particulate matter to precursor emissions, Atmos. Environ., 44, 3719-3727, 2010.
Nenes, A., Pilinis, C., and Pandis, S.N.: Continued development and testing of a new thermodynamic aerosol module for urban and regional air quality models, Atmos. Environ., 33, 1553-1560, 1999.
Nie, T., Li, X., Wang, X., Shao, M., and Zhang, Y.: Characteristics of the Spatial Distributions of Ozone-Precursor Sensitivity Regimes in Summer over Beijing, Acta Scientiarum Naturalium Universitatis Pekinensis, 50(3), 557-564, 2014. (in Chinese)
Olivier, J., Bouwman, A., Maas, C., and Berdowski, J.: Emission database for global atmospheric research, Environ. Monit. Assess., 31, 93-106., 1994.
Ran, L., Zhao, C., Xu, W., Han, M., Lu, X., Han, S., Lin, W., Xu, X., Gao, W., Yu, Q., Geng, F., Ma, N., Deng, Z., and Chen, J.: Ozone production in summer in the megacities of Tianjin and Shanghai, China: a comparative study, Atmos. Chem. Phys., 12, 7531-7542, 2012.
Sarwar, G., Luecken, D., Yarwood, G., Whitten, G. Z., Carter, W. P. L.: Impact of an updated carbon bond mechanism on predictions from the CMAQ modeling system: preliminary assessment, J. Appl. Meteor. Climatol., 47, 3-14, 2008.
Sillman, S. and He, D.: Some theoretical results concerning O_3-NO_x-VOC chemistry and NO_x-VOC indicators, J. Geophys. Res., 107(D22): ACH-1-ACH 26-15, 2002.
Sillman, S. and West, J.: Reactive nitrogen in Mexico City and its relation to ozone-precursorsensitivity: results from photochemical models, Atmos. Chem. Phys., 9, 3477-3489, 2009.
Streets, D., Bond, T., Carmichael, G., Fernandes, S., Fu, Q., He, D., Klimont, Z., Nelson, S. M., Tsai, N. Y., Wang, : An inventory of gaseous and primary aerosol emissions in Asia in the year 2000, J. Geophys. Res., 108, DOI: 10.1029/2002JD003093, 2003.
Tang, G., Wang, Y., Li, X., Ji, D., Hsu, S., Gao, X.: Spatial-temporal variations in surface ozone in Northern China as observed during 2009–2010 and possible implications for future air quality control strategies, Atmos. Chem. Phys., 12, 2757-2776, 2012.
Tang, G., Zhu, X., Xin, J., Hu, B., Tao, S., Sun, Y., Zhang, J., Wang, L., Cheng, M., Chao, N., Kong, L., Li, X., and Wang, Y.: Modelling study of boundary-layer ozone over northern China - Part I: Ozone budget in summer, Atmos. Res., 187, 128-137, 2017.
Tao, M., Chen, L., Su, L., and Tao, J.: Satellite observation of regional haze pollution over the North China Plain, J. Geophys. Res., 117, D12203, doi:10.1029/2012JD017915, 2012.
van der Werf, G. R., Randerson, J. T., Giglio, L., Collatz, G. J., Mu, M., Kasibhatla, P. S., Morton, D. C., DeFries, R. S., Jin, Y., van Leeuwen, T. T.: Global fire emissions and the contribution of deforestation, savanna, forest, agricultural, and peat fires (1997-2009), Atmos. Chem. Phys., 10, 11707-11735, 2010.
Wang, X., Sun, M., Yang, T., and Wang, Z.: Interdecadal change in frequency of dust-haze episodes in North China Plain, Clim. Environ. Res., 18, 165–170, 2013 (in Chinese).
Wang, Y., Konopka, P., Liu, Y., Chen, H., Muller, R., Ploger, F., Riese, M., Cai, Z., and Lu, D.: Tropospheric ozone trend over Beijing from 2002–2010: ozonesonde measurements and modeling analysis, Atmos. Chem. Phys., 12, 8389-8399, 2010.

Wang, Z. S., Chien, C. J., Tonnesen, G. S.: Development of a tagged species source apportionment algorithm to characterize three-dimensional transport and transformation of precursors and secondary pollutants, J. Geophys. Res., 114, D21. DOI: 10.1029/2008JD010846, 2009.

Wu, R. and Xie, S.: Spatial Distribution of Ozone Formation in China Derived from Emissions of Speciated Volatile Organic Compounds, Environ. Sci. Technol., 51(5), 2574-2583, 2017.

Xing, J., Wang, S., Zhu, Y.: Nonlinear response of ozone to precursor emission Changes in China: A modeling study using response surface methodology, Atmos. Chem. Phys., 11(10):5027-5044, 2010.

Yang, Y., Wilkinson, J., and Russell, A.: Fast, direct sensitivity analysis of multi-dimensional photochemical models, Environ. Sci. Technol., 31(10), 2859–2868, 1997.

Yu, S. C., Eder, B., Dennis, R., Chu, S. H., and Schwartz, S.: New unbiased symmetric metrics for evaluation of air quality models, Atmos. Sci. Lett., 7, 26–34, 2006.

Yu, S., Mathur, R., Sarwar, G., Kang, D., Tong, D., Pouliot, G. and Pleim, J.: Eta-CMAQ air quality forecasts for O_3 and related species using three different photochemical mechanisms (CB4, CB05, SAPRC-99): comparisons with measurements during the 2004 ICARTT study, Atmos. Chem. Phys., 10, 3001–3025, 2010.

Zhang, M., Uno, I., Zhang, R., Han, Z., Wang, Z., and Pu, Y.: Evaluation of the Models-3 Community Multi-scale Air Quality (CMAQ) modeling system with observations obtained during the TRACE-P experiment: comparison of ozone and its related species, Atmos. Environ., 40, 4874-4882, 2006.

Zhou, S., Yang, L., Gao, R., Wang, X., Gao, X., Nie, W., Xu, P., Zhang, Q., and Wang, W.: A comparison study of carbonaceous aerosols in a typical North China Plain urban atmosphere: Seasonal variability, sources and implications to haze formation, Atmos. Environ., 149, 95-103, 2017.

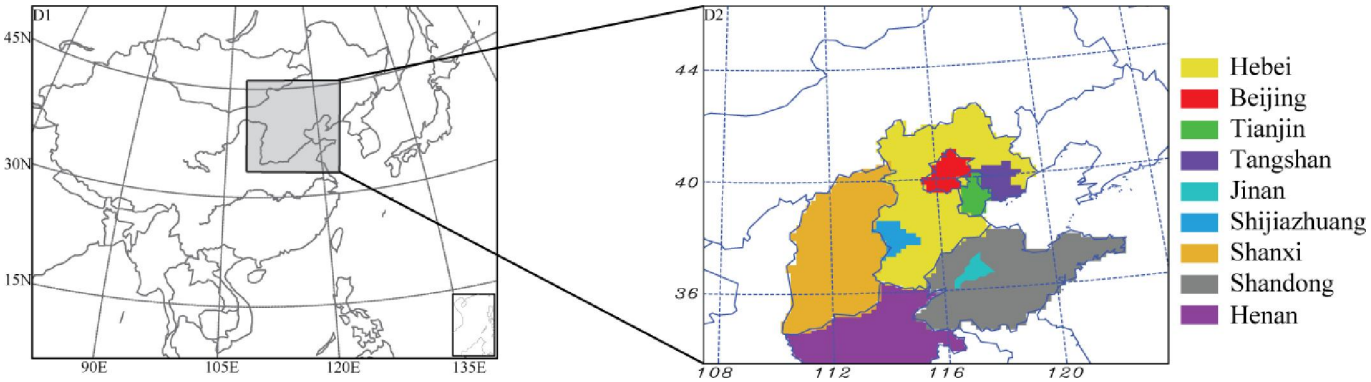

Figure 1 The model domain of this study, and the geographic locations of Beijing, Tianjin, Tangshan, Hebei, Shijiazhuang, Shanxi, Shandong, Jinan, and Henan.

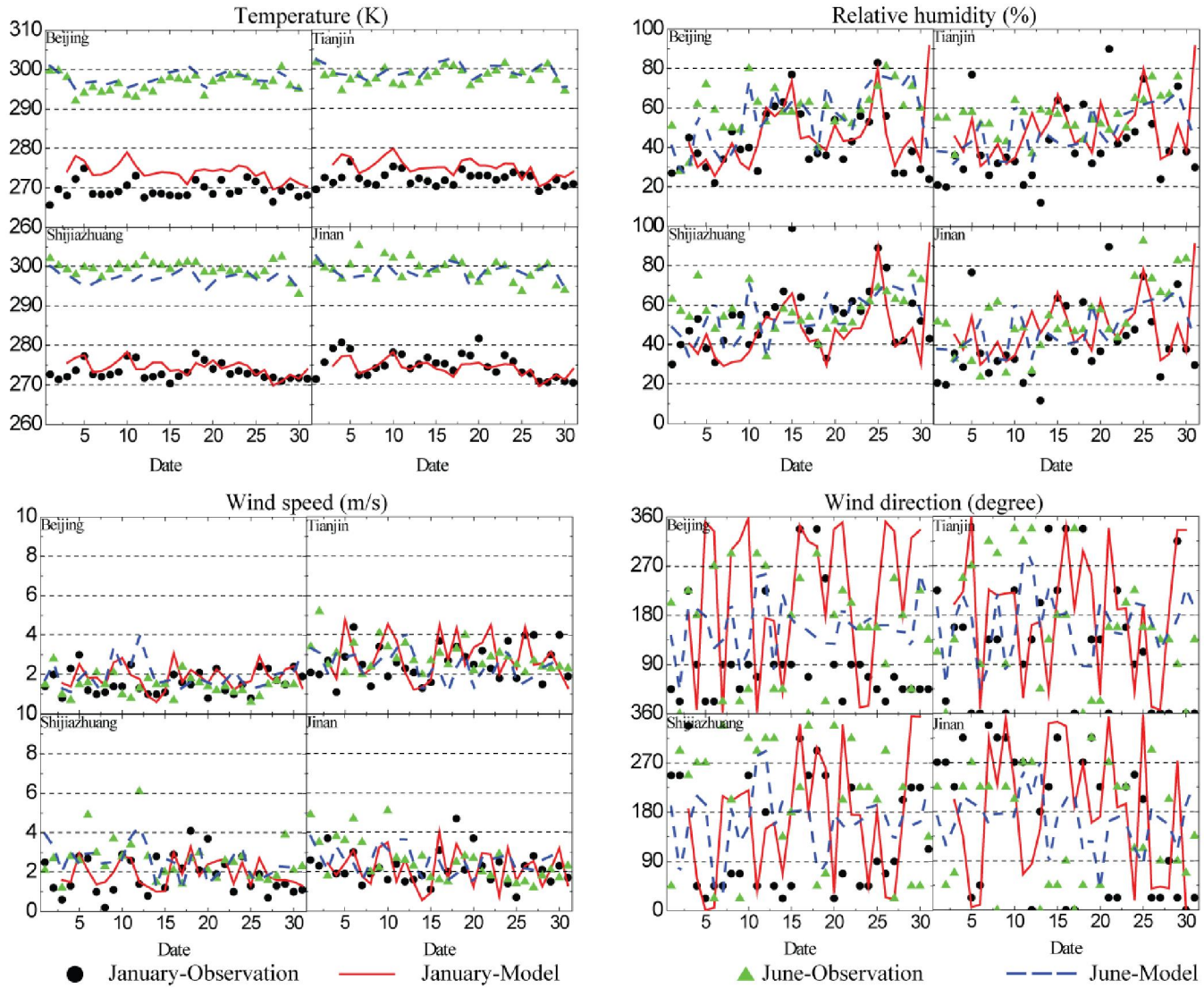

Figure 2.Observed and modeled daily average temperatures (K), relative humidity (%), wind speed (m/s), and maximum wind direction at four stations in January and June 2015.

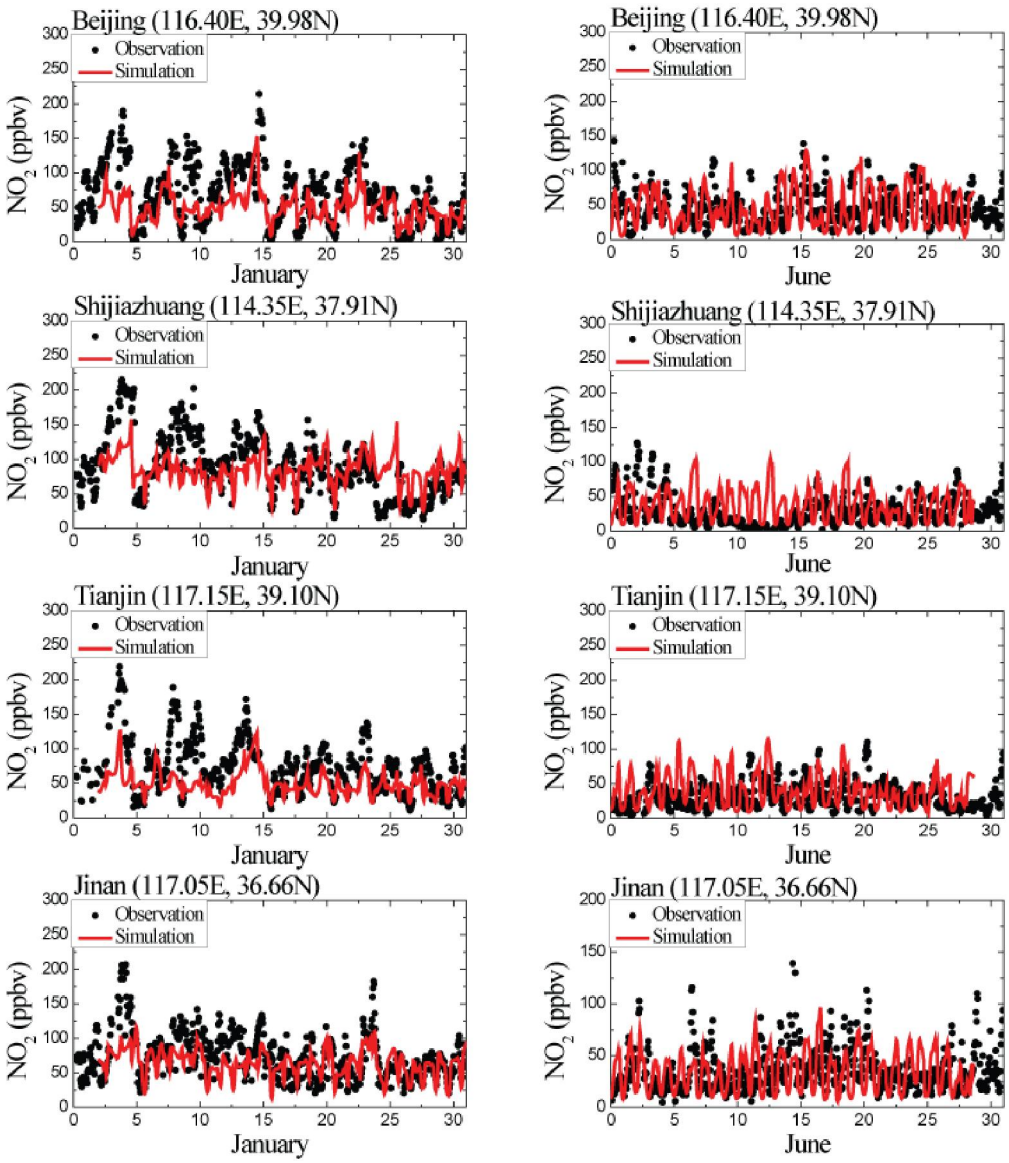

Figure 3. Observed (black circles) and modeled (red solid lines) hourly mass concentrations (μg m^{-3}) of NO_2 at Beijing, Shijiazhuang, Tianjin, and Jinan in January and June 2015.

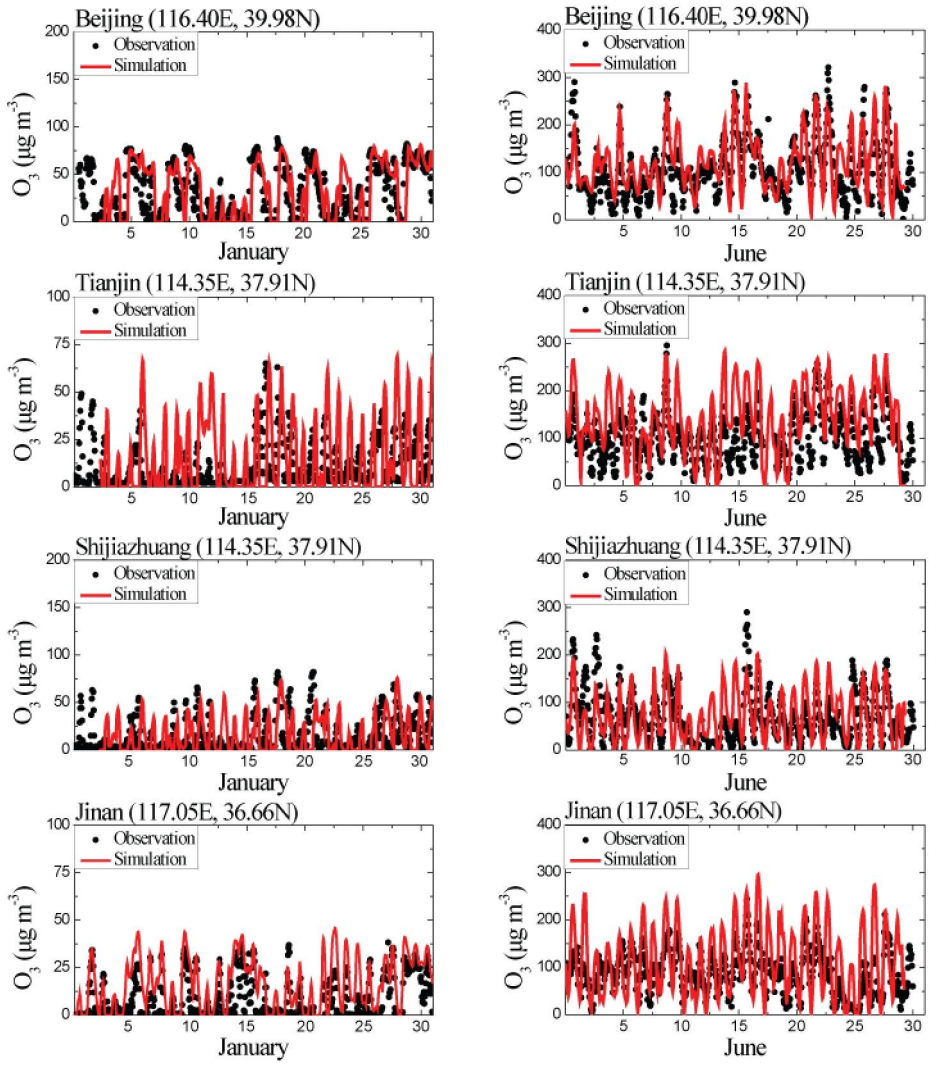

Figure 4. Observed (black circles) and modeled (red solid lines) hourly mass concentrations (μg m^{-3}) of O_3 at Beijing, Shijiazhuang, Tianjin, and Jinan in January and June 2015.

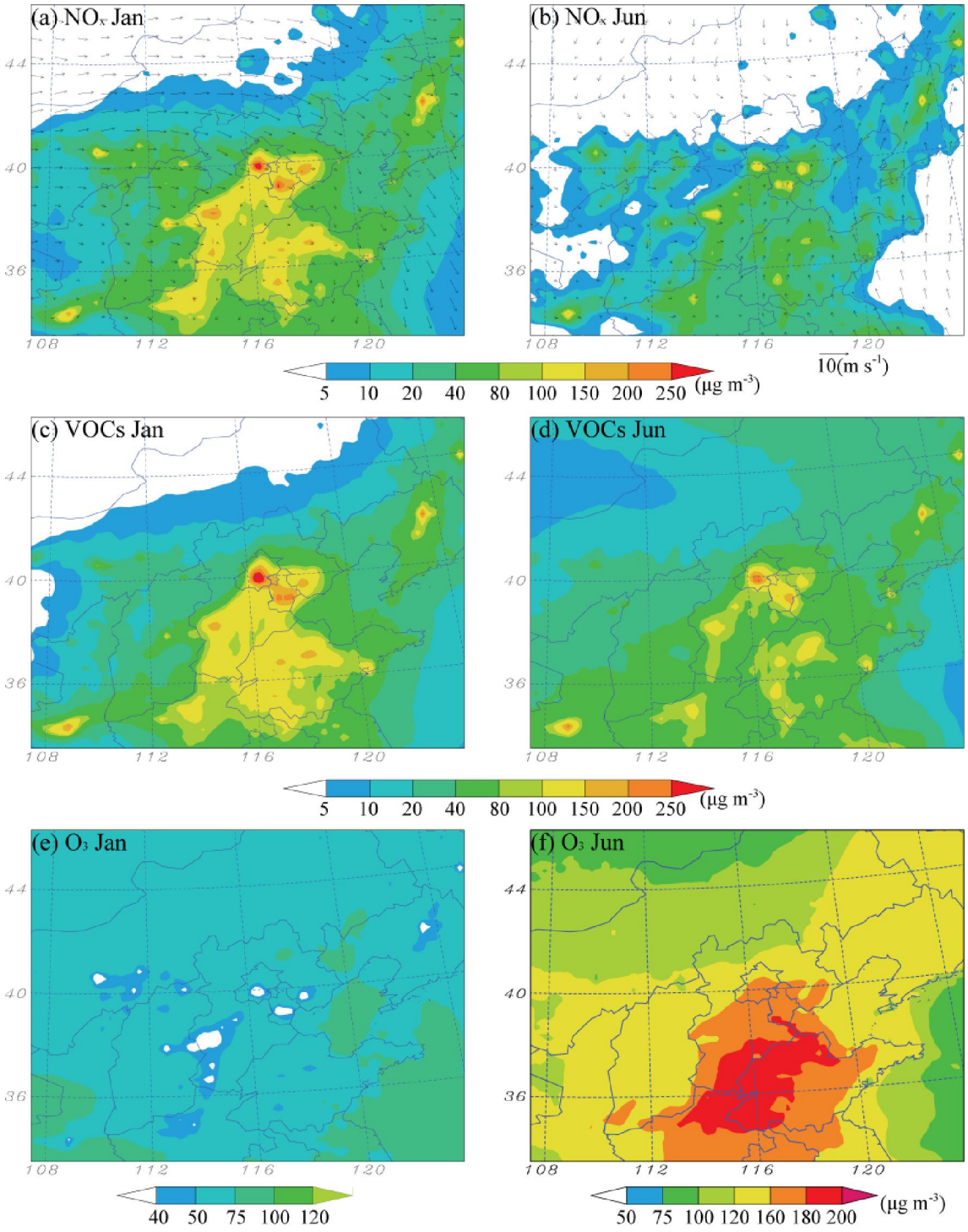

Figure 5. The surface spatial distributions of monthly average NO_x (a-b) and VOCs (c-d), and maximum daily 8H-O_3 (e-f) in January and June 2015.

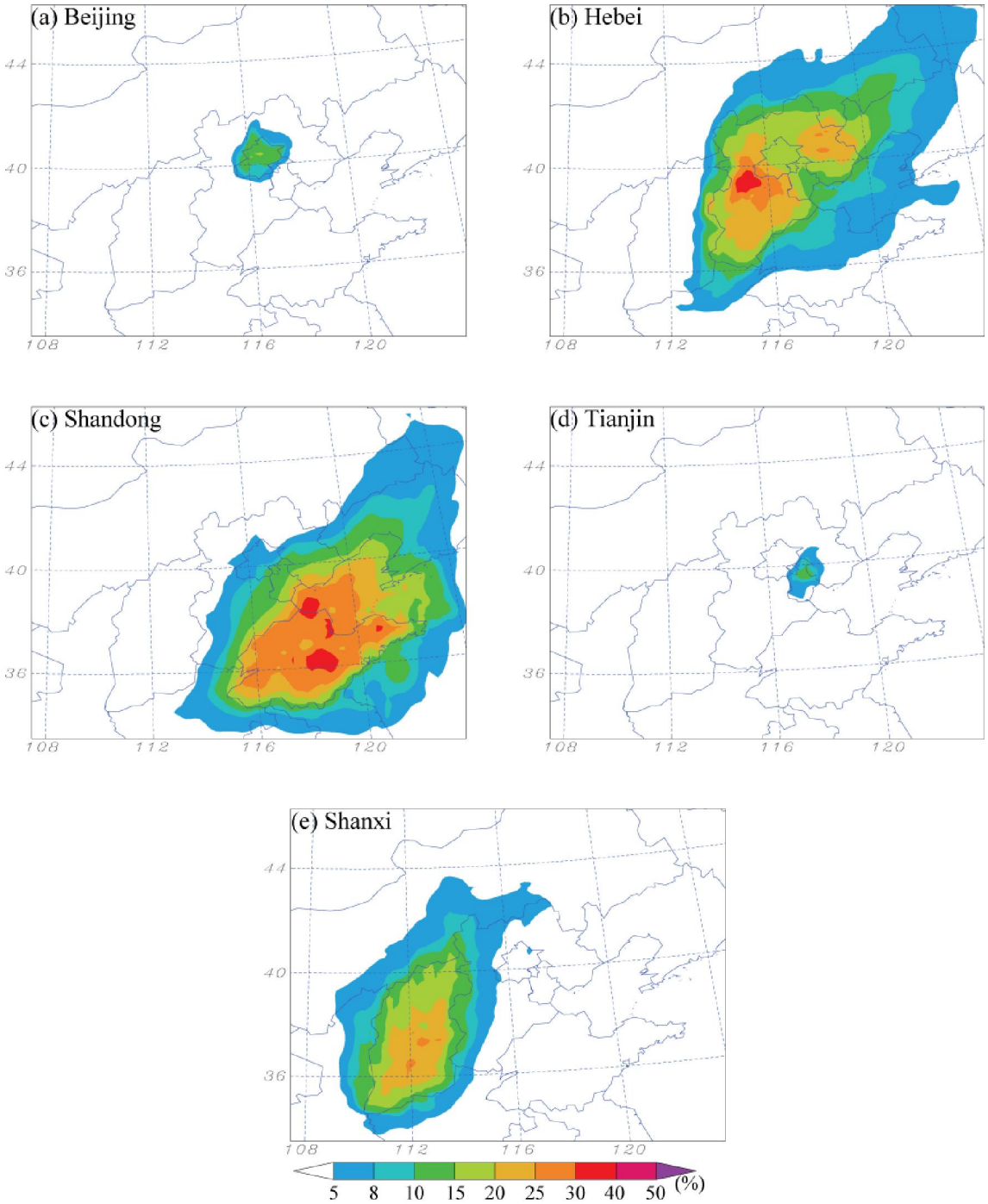

Figure 6. The regional contribution of NO_x-sensitive O_3 from (a) Beijing, (b) Hebei, (c) Shandong, (d) Tianjin, and (e) Shanxi in June 2015.

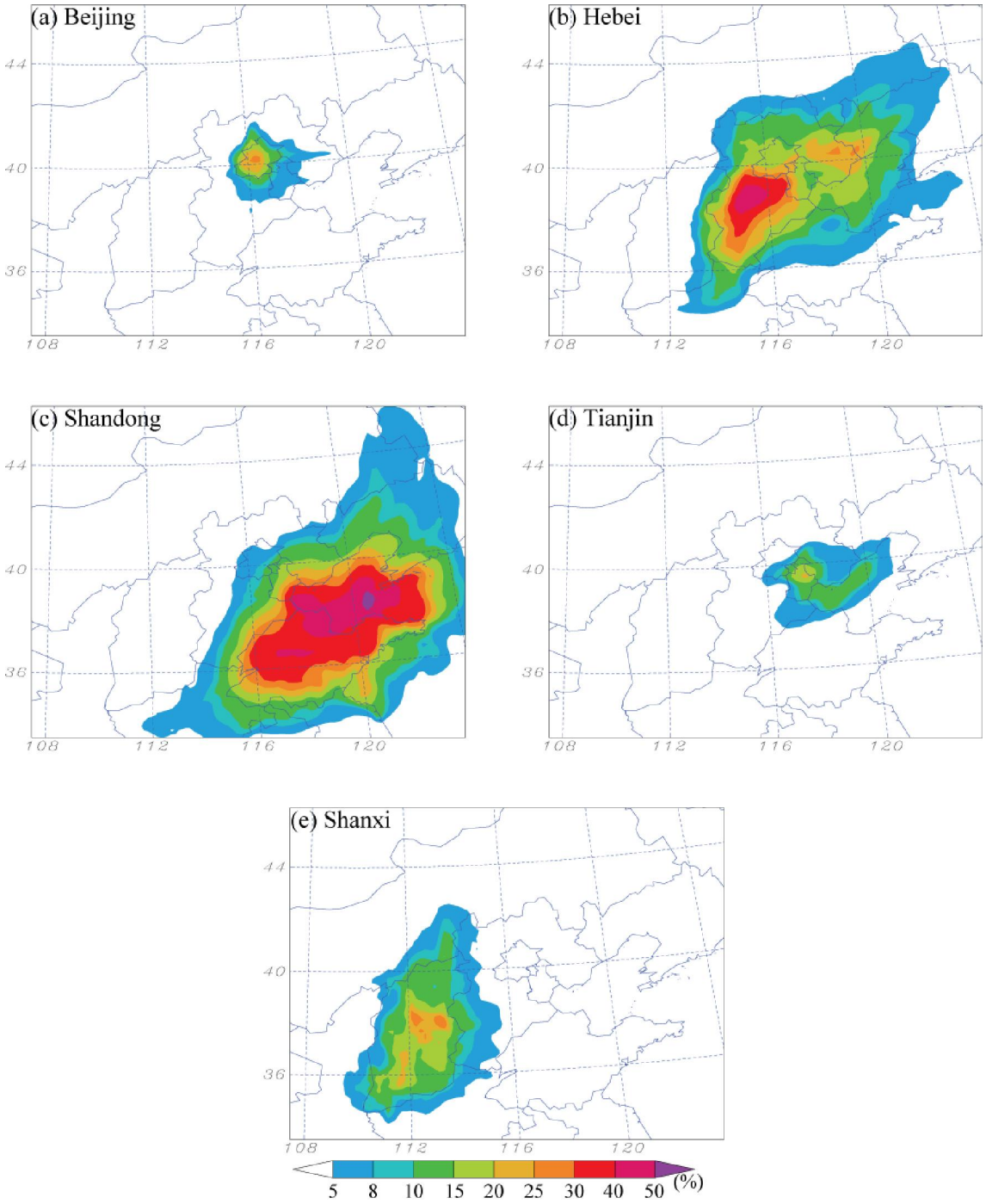

Figure 7.Same as Figure 5 but for VOC-sensitive O_3.

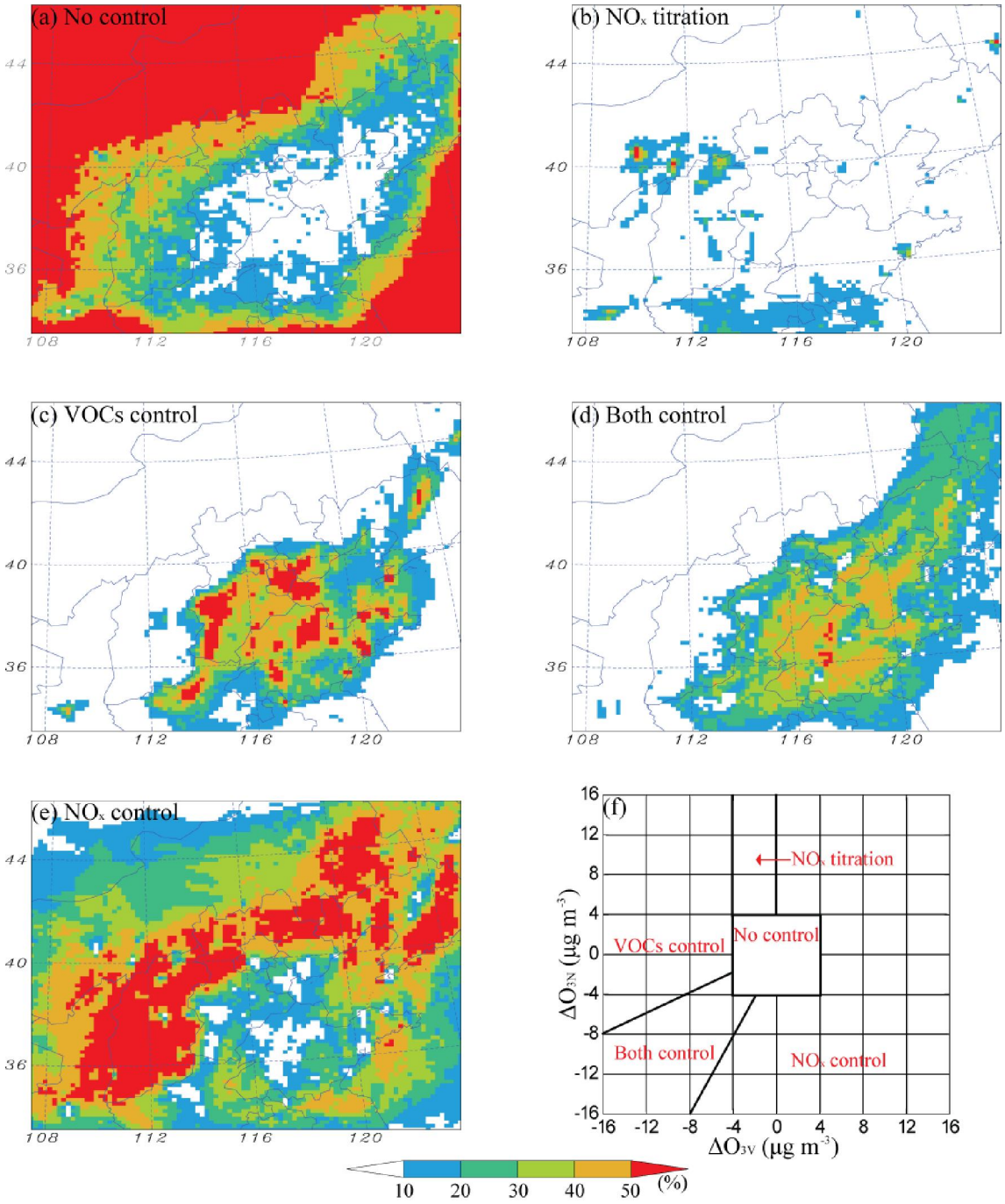

Figure 8. Distributions of the frequency of 8-hour ozone precursor sensitivity regions in June 2015.

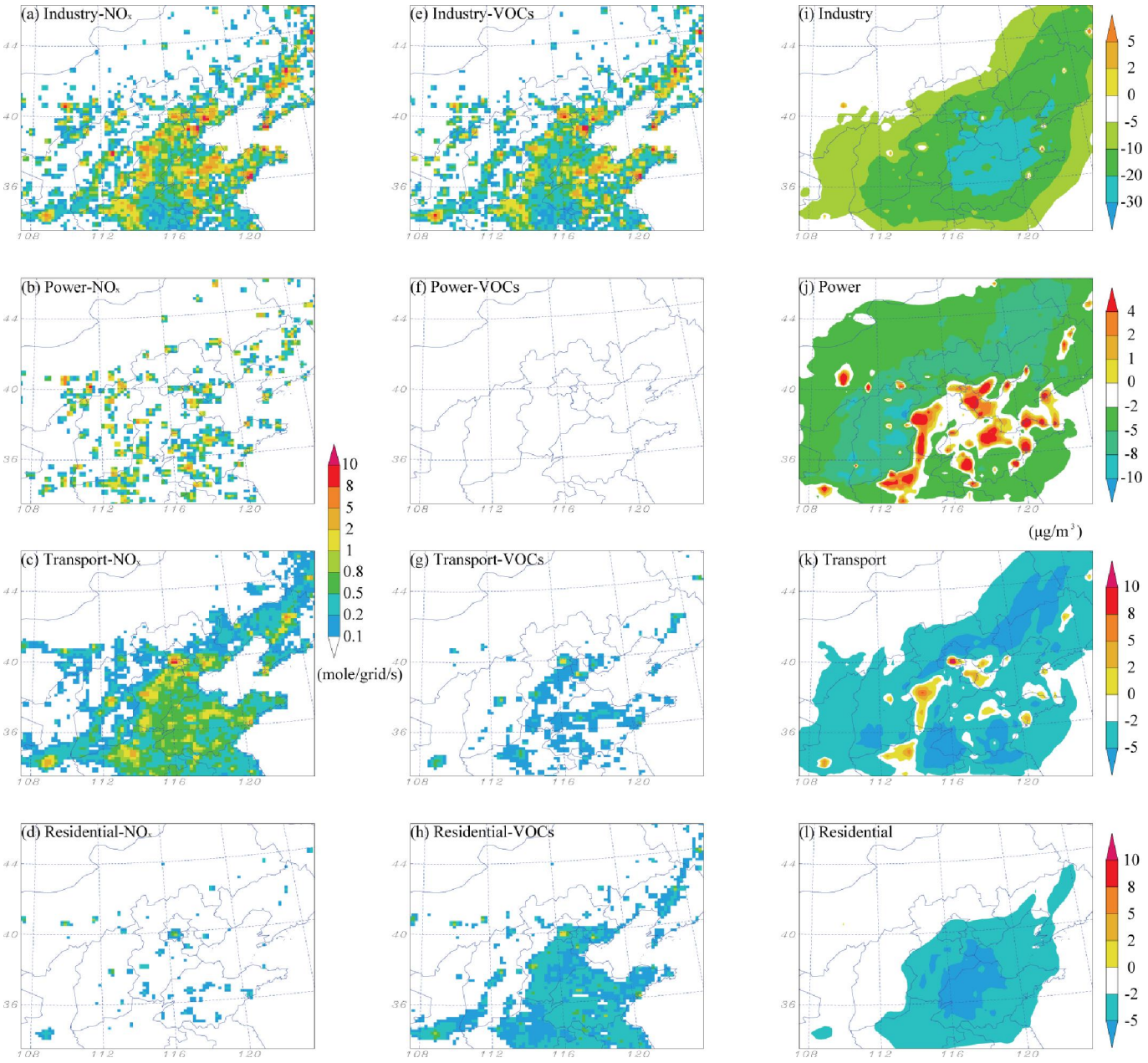

Figure 9. Distributions of the emission flux of NO_x and VOCs and the variation of mass concentration of 8H-O_3 associated with the ZI, ZP, ZT, and ZR in June.

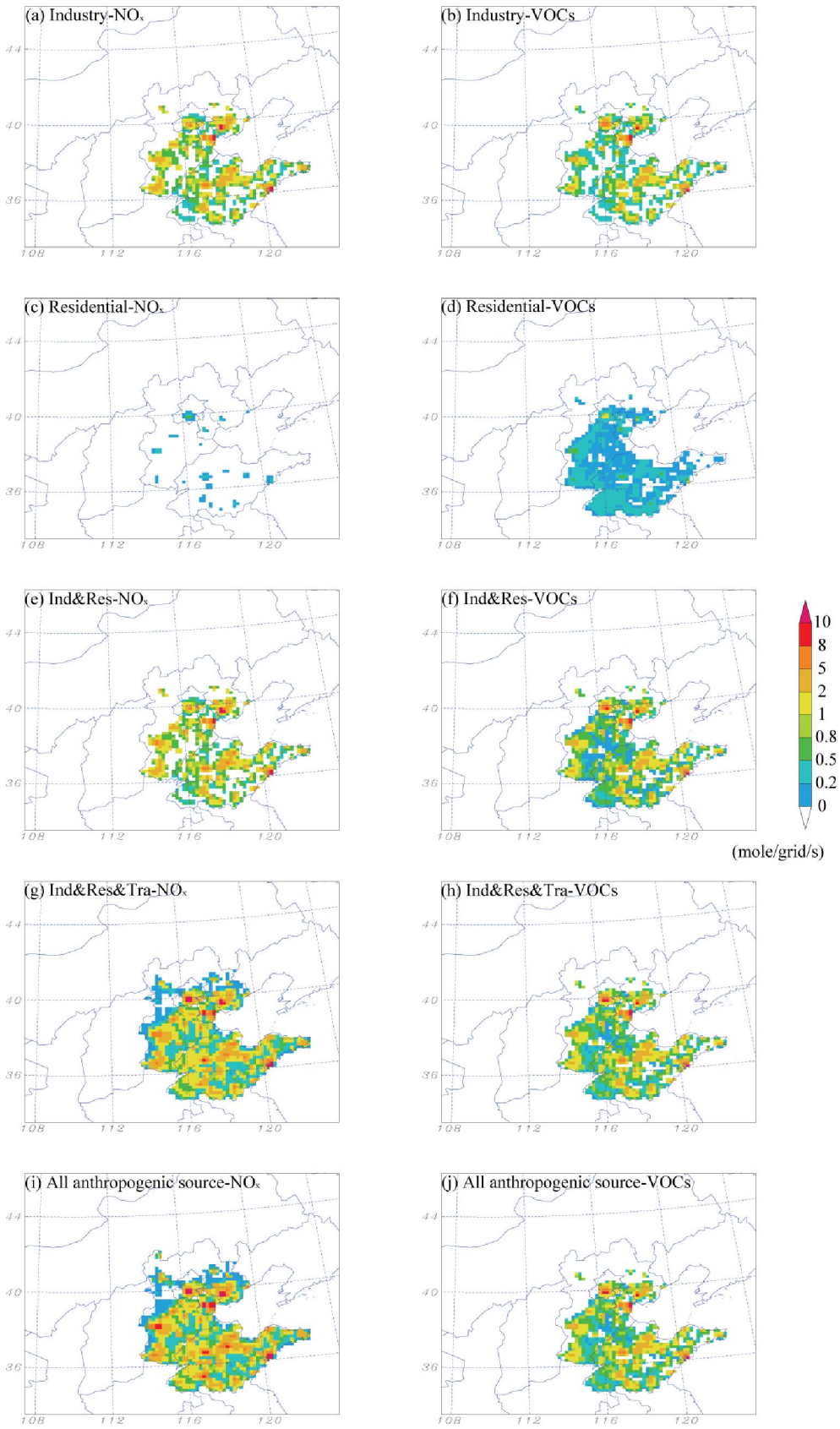

Figure 10. Distributions of the NO_x and VOCs emission flux from different sectors or combinations in the high emission regions of Beijing, Tianjin, Hebei, Shandong in June.

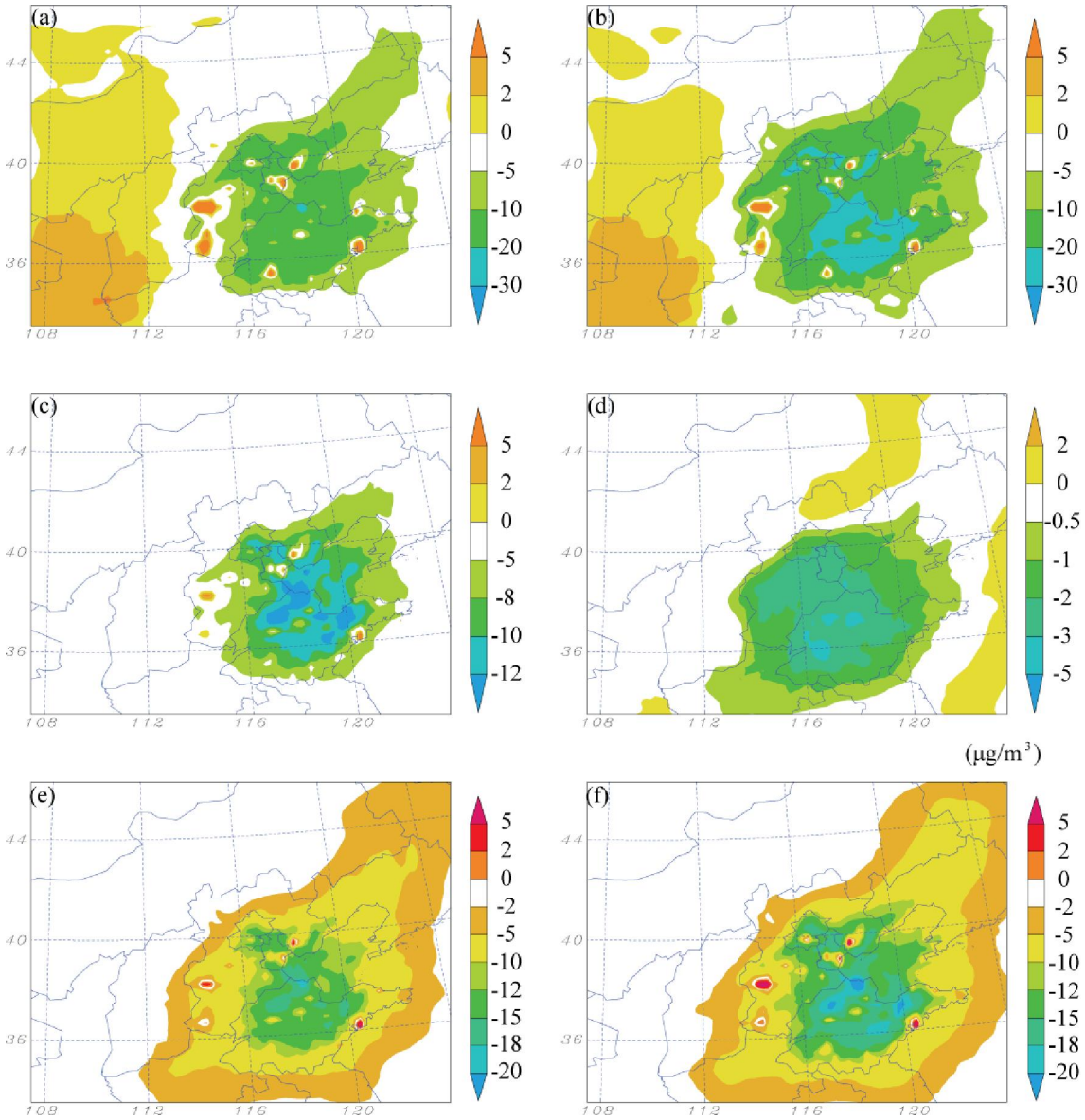

Figure 11. Distributions of the variation of 8H-O_3 mass concentration associated with brute force sensitivity tests: (a) A20%-HER; (b) A20%-BHTS; (c) I20%-HER; (d) R20%-HER; (e) IR20%-HER; (f) ITR20%-HER.

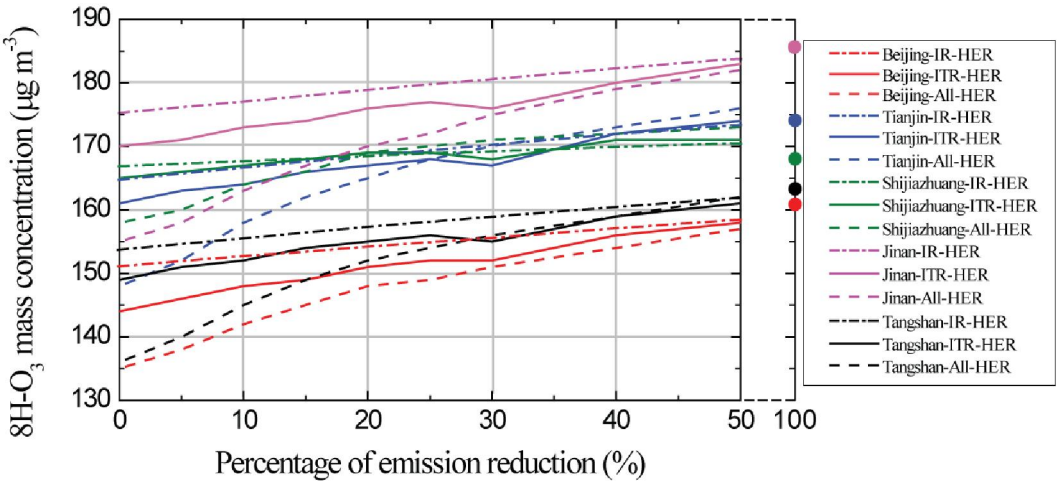

Figure 12. The variation of regional average 8H-O_3 mass concentrations in Beijing, Tianjin, Shijiazhuang, Jinan, and Tangshan with reduction of IR, ITR and All emissions, respectively.

Table 1. Statistical summary of the comparisons of the hourly NO_2 comparison between simulation and observation

			N[a]	C_{obs}[b]	C_{mod}[c]	σ_{obs}[d]	σ_{mod}[e]	R[f]
NO_2	Beijing	Jan	602	68.71	50.62	42.98	21.7	0.59
		Jun	588	45.39	46.75	24.95	28.49	0.53
	Jinan	Jan	616	74.39	63.26	33.98	19.55	0.55
		Jun	639	34.27	34.93	19.57	18.76	0.47
	Shijiazhuang	Jan	618	90.04	83.78	44.91	21.55	0.54
		Jun	629	26.11	38.82	21.59	22.26	0.44
	Tianjin	Jan	584	73.73	49.07	37.94	18.52	0.55
		Jun	639	30.02	40.29	18.36	23.25	0.52

[a] Number of samples

[b] Total mean of observation

[c] Total mean of simulation

[d] Standard deviation of observation

[e] Standard deviation of simulation

[f] Correlation coefficient between daily observation and simulation

Table 2. Statistical summary of the comparisons of the hourly O_3 comparison between simulation and observation

			N	C_{obs}	C_{mod}	σ_{obs}	σ_{mod}	R
O_3	Beijing	Jan	615	33.57	37.88	27.58	27.2	0.54
		Jun	676	106.96	120.85	63.75	57.33	0.74
	Jinan	Jan	673	11.09	13.58	10.75	13.08	0.74
		Jun	693	87.91	111.44	45.54	71.8	0.62
	Shijiazhuang	Jan	627	15.24	18.54	18.74	18.7	0.57
		Jun	692	69.53	71.78	53.15	76.14	0.65
	Tianjin	Jan	629	10.83	17.05	11.78	19.36	0.48
		Jun	675	100.42	143.31	52.22	69.48	0.74

Table 3. The regional transport contributions of O_3 mass concentration in Beijing, Tianjin, Hebei, Shandong, Shanxi, and boundary condition (BCON), initial condition (ICON), and other sources (nature sources)

	Beijing	Tianjin	Hebei	Shandong	Shanxi	BCON	ICON	Other
Beijing	23.1%	5.3%	35.2%	13.2%	5.4%	7.3%	0.1%	10.4%
Tianjin	9.0%	14.9%	29.0%	37.3%	3.6%	1.8%	0.1%	4.3%
Hebei	6.3%	5.3%	36.6%	19.4%	7.7%	16.4%	0.1%	8.2%
Shandong	1.3%	2.1%	9.6%	53.6%	3.1%	19.4%	0.1%	10.8%
Shanxi	1.4%	1.4%	10.8%	4.5%	45.0%	22.1%	0.1%	14.7%

888 Table 4. The brute force sensitivity tests set in this study

	Abbreviation	Brute force sensitivity test
1	ZI	Zero-out of industry emission sector
2	ZP	Zero-out of power plants emission sector
3	ZT	Zero-out of transport emission sector
4	ZR	Zero-out of residential emission sector
5	A20%-BHTS	20% emission of all anthropogenic sectors in BTHS
6	A20%-HER	20% emission of all anthropogenic sectors in the selected high emission regions of BTHS
7	I20%-HER	20% emission of industry sector in the selected high emission regions of BTHS
8	R20%-HER	20% emission of residential sector in the selected high emission regions of BTHS
9	IR20%-HER	20% emission of industry and residential sector in the selected high emission regions of BTHS
10	ITR20%-HER	20% emission of industry, transport, and residential sector in the selected high emission regions of BTHS

889
890
891
892
893
894
895
896
897
898
899
900
901
902
903
904
905
906
907
908
909
910
911
912
913
914
915

916
917
918
919
920
921
922
923
924
925
926
927
928